

# Influence of energy-transfer upconversion and excited-state absorption on a high power Nd:YVO<sub>4</sub> laser at 1.34 μm

YAYUN MA,<sup>1</sup> YUANJI LI,<sup>1,2</sup> JINXIA FENG,<sup>1,2</sup> AND KUANSHOU ZHANG<sup>1,2,\*</sup>

<sup>1</sup>State Key Laboratory of Quantum Optics and Quantum Optics Devices, Institute of Opto-Electronics, Shanxi University, Taiyuan 030006, China

<sup>2</sup>Collaborative Innovation Center of extreme Optics, Shanxi University, Taiyuan 030006, China

\*kuanshou@sxu.edu.cn

**Abstract:** A self-consistent theoretical model considering both energy-transfer upconversion (ETU) and excited-state absorption (ESA) effects, as well as the couplings among the temperature distribution in the laser crystal, the thermal fractional loading, the upper state population involved in the ETU and ESA effects, the laser output and other temperature-dependent parameters, was developed to simulate the behaviors of diode-end-pumped continuous-wave (CW) single-transverse-mode (TEM<sub>00</sub>) lasers. Based on the theoretical and experimental investigations of the influences of ETU and ESA effects on laser performance, a high power CW TEM<sub>00</sub> Nd:YVO<sub>4</sub> 1.34 μm laser dual-end pumped at 880 nm was achieved with a maximum output power of 16 W. The measured laser beam quality was  $M_x^2 = M_y^2 = 1.17$  and the stability of the laser output was better than  $\pm 0.9\%$  in a given four hours. The theoretical predictions considering both ETU and ESA effects are in good agreement with experimental results.

© 2018 Optical Society of America under the terms of the [OSA Open Access Publishing Agreement](#)

**OCIS codes:** (140.3460) Lasers; (140.3480) Lasers, diode-pumped; (140.3613) Lasers, upconversion; (140.6810) Thermal effects.

## References and links

1. M. Milanič and B. Majaron, "Energy deposition profile in human skin upon irradiation with a 1,342 nm Nd:YAP laser," *Lasers Surg. Med.* **45**(1), 8–14 (2013).
2. M. R. Huo, J. L. Qin, Z. H. Yan, X. J. Jia, and K. C. Peng, "Generation of two types of nonclassical optical states using an optical parametric oscillator with a PPKTP crystal," *Appl. Phys. Lett.* **109**(22), 221101 (2016).
3. Y. Yan, H. Zhang, Y. Liu, X. Yu, H. Zhang, J. He, and J. Xin, "Near-diffraction-limited, 35.4 W laser-diode end-pumped Nd:YVO<sub>4</sub> slab laser operating at 1342 nm," *Opt. Lett.* **34**(14), 2105–2107 (2009).
4. L. Fornasiero, S. Kück, T. Jensen, G. Huber, and B. H. T. Chai, "Excited state absorption and stimulated emission of Nd<sup>3+</sup> in crystals. Part 2: YVO<sub>4</sub>, GdVO<sub>4</sub>, and Sr<sub>5</sub>(PO<sub>4</sub>)<sub>3</sub>F," *Appl. Phys. B* **67**(5), 549–553 (1998).
5. Y. F. Chen, L. J. Lee, T. M. Huang, and C. L. Wang, "Study of high-power diode-end-pumped Nd:YVO<sub>4</sub> laser at 1.34 μm: influence of Auger upconversion," *Opt. Commun.* **163**(4–6), 198–202 (1999).
6. M. Okida, M. Itoh, T. Yatagai, H. Ogilvy, J. Piper, and T. Omatsu, "Heat generation in Nd doped vanadate crystals with 1.34 μm laser action," *Opt. Express* **13**(13), 4909–4915 (2005).
7. Y. T. Chang, Y. P. Huang, K. W. Su, and Y. F. Chen, "Comparison of thermal lensing effects between single-end and double-end diffusion-bonded Nd:YVO<sub>4</sub> crystals for <sup>4</sup>F<sub>3/2</sub>→<sup>4</sup>I<sub>11/2</sub> and <sup>4</sup>F<sub>3/2</sub>→<sup>4</sup>I<sub>13/2</sub> transitions," *Opt. Express* **16**(25), 21155–21160 (2008).
8. F. Lenhardt, M. Nittmann, T. Bauer, J. Bartschke, and J. A. L'huillier, "High-power 888-nm-pumped Nd:YVO<sub>4</sub> 1342-nm oscillator operating in the TEM<sub>00</sub> mode," *Appl. Phys. B* **96**(4), 803–807 (2009).
9. B. Li, X. Ding, B. Sun, Q. Sheng, J. Liu, Z. Wei, P. Jiang, C. Fan, H. Zhang, and J. Yao, "12.45 W wavelength-locked 878.6 nm laser diode in-band pumped multisegmented Nd:YVO<sub>4</sub> laser operating at 1342 nm," *Appl. Opt.* **53**(29), 6778–6781 (2014).
10. O. Guillot-Noël, A. Kahn-Harari, B. Viana, D. Vivien, E. Antic-Fidancev, and P. Porcher, "Optical spectra and crystal field calculations of Nd<sup>3+</sup> doped zircon-type YMO<sub>4</sub> laser hosts (M = V, P, As)," *J. Phys. Condens. Matter* **10**(29), 6491–6503 (1998).
11. Y. F. Chen, Y. P. Lan, and S. C. Wang, "Influence of energy-transfer upconversion on the performance of high-power diode-end-pumped CW lasers," *IEEE J. Quantum Electron.* **36**(5), 615–619 (2000).
12. Y. Guyot and R. Moncorge, "Excited-state absorption in the infrared emission domain of Nd<sup>3+</sup>-doped Y<sub>3</sub>Al<sub>5</sub>O<sub>12</sub>, YLiF<sub>4</sub>, and LaMgAl<sub>11</sub>O<sub>19</sub>," *J. Appl. Phys.* **73**(12), 8526–8530 (1993).

13. X. Yan, Q. Liu, L. Huang, Y. Wang, X. Huang, D. Wang, and M. Gong, "A high efficient one-end-pumped TEM<sub>00</sub> laser with optimal pump mode," *Laser Phys. Lett.* **5**(3), 185–188 (2008).
14. S. Bjurshagen and R. Koch, "Modeling of energy-transfer upconversion and thermal effects in end-pumped quasi-three-level lasers," *Appl. Opt.* **43**(24), 4753–4767 (2004).
15. M. D. Wei, Y. S. Lai, and K. C. Chang, "Generation of a radially polarized laser beam in a single microchip Nd:YVO<sub>4</sub> laser," *Opt. Lett.* **38**(14), 2443–2445 (2013).
16. M. Sabaean, H. Nadgaran, and L. Mousave, "Analytical solution of the heat equation in a longitudinally pumped cubic solid-state laser," *Appl. Opt.* **47**(13), 2317–2325 (2008).
17. Y. Wang, W. Yang, H. Zhou, M. Huo, and Y. Zheng, "Temperature dependence of the fractional thermal load of Nd:YVO<sub>4</sub> at 1064 nm lasing and its influence on laser performance," *Opt. Express* **21**(15), 18068–18078 (2013).
18. N. Ter-Gabrielyan, V. Fromzel, and M. Dubinskii, "Linear thermal expansion and thermo-optic coefficients of YVO<sub>4</sub> crystals the 80–320 K temperature range," *Opt. Mater. Express* **2**(11), 1624–1631 (2012).
19. D. E. Zelmon, J. J. Lee, K. M. Currin, J. M. Northridge, and D. Perlov, "Revisiting the optical properties of Nd doped yttrium orthovanadate," *Appl. Opt.* **49**(4), 644–647 (2010).
20. G. Turri, H. P. Jentsen, F. Cornacchia, M. Tonelli, and M. Bass, "Temperature-dependent stimulated emission cross section in Nd<sup>3+</sup>:YVO<sub>4</sub> crystals," *J. Opt. Soc. Am. B* **26**(11), 2084–2088 (2009).
21. Y. G. Zhao, H. H. Yu, Z. P. Wang, H. J. Zhang, X. G. Xu, and J. Y. Wang, "Homogeneous and inhomogeneous spectrum broadening in Nd<sup>3+</sup>-doped mixed vanadate crystals," *Opt. Mater.* **71**, 78–85 (2017).
22. N. A. Tolstik, G. Huber, V. V. Maltsev, N. I. Leonyuk, and N. V. Kuleshov, "Excited state absorption, energy levels, and thermal conductivity of Er<sup>3+</sup>:YAB," *Appl. Phys. B* **92**(4), 567–571 (2008).
23. M. Laroche, S. Girard, J. K. Sahu, W. A. Clarkson, and J. Nilsson, "Accurate efficiency evaluation of energy-transfer processes in phosphosilicate Er<sup>3+</sup>-Yb<sup>3+</sup>-codoped fibers," *J. Opt. Soc. Am. B* **23**(2), 195–202 (2006).
24. P. Shi, W. Chen, L. Li, and A. Gan, "Semi-analytical thermal analysis of thermal focal length on Nd:YAG rods," *Appl. Opt.* **46**(26), 6655–6661 (2007).
25. Y. J. Shen, M. L. Gong, E. C. Ji, X. Fu, and L. C. Sun, "Spatial dynamic thermal iteration model for 888 nm end-pumped Nd:YVO<sub>4</sub> solid-state laser oscillators and amplifiers," *Opt. Commun.* **383**, 430–440 (2017).

## 1. Introduction

Solid state neodymium lasers operating around 1.34  $\mu\text{m}$  have received great attention because of their numerous practical applications, such as fiber telecommunication, fiber sensing, medical treatment and scientific research [1,2]. Diode-end-pumped Nd:YVO<sub>4</sub> laser system corresponding to the  ${}^4F_{3/2}$  to  ${}^4I_{13/2}$  transition is the most frequently used method for generating 1.34  $\mu\text{m}$  laser with high output and good beam quality [3]. Comparing with Nd:YVO<sub>4</sub> lasers operating at 1.06  $\mu\text{m}$ , 1.34  $\mu\text{m}$  lasers suffer from more serious thermal effects and usually exhibit lower conversion efficiency. These phenomena can be attributed to two reasons: (i) for the 1.34  $\mu\text{m}$  emission and 808 nm pump source, the quantum defect of 39.8% is larger than that of 24% for 1.06  $\mu\text{m}$  emission; (ii) owing to the energy level resonance and small stimulated emission cross-section at 1.34  $\mu\text{m}$ , some detrimental energy processes, such as the excited state absorption (ESA) and the energy transfer upconversion (ETU) will play an important role in the generation of 1.34  $\mu\text{m}$  lasers [4,5]. Fornasiero *et al.* measured ESA of the Nd:YVO<sub>4</sub> crystal and showed that ESA is a small loss factor to the laser emission near 1.06  $\mu\text{m}$ , but does considerably diminish the effective emission cross-sections near 1.34  $\mu\text{m}$  [4]. Okida *et al.* investigated the thermal load in Nd:YVO<sub>4</sub> crystal with and without laser action at 1.34  $\mu\text{m}$  and came to a conclusion that ESA contributes significantly to a fractional thermal loading as well as quantum defect [6]. Chen *et al.* studied the influence of ETU on a high-power diode-end-pumped Nd:YVO<sub>4</sub> laser at 1.34  $\mu\text{m}$  [5]. They gave results that the strong dependence of the slope efficiency of 1.34  $\mu\text{m}$  laser on the Nd<sup>3+</sup> doping concentration is attributed to the ETU process, and the ETU induced population reduction can be circumvented using low-doped crystals. Chang *et al.* compared thermal lensing effects between single-end and double-end diffusion-bonded Nd:YVO<sub>4</sub> crystals for  ${}^4F_{3/2} \rightarrow {}^4I_{13/2}$  transition and found using a double-end diffusion-bonded crystal can mitigate the strong thermal lensing effect [7]. Lenhardt *et al.* obtained a high-power single-transverse-mode (TEM<sub>00</sub>) Nd:YVO<sub>4</sub> 1.34  $\mu\text{m}$  laser by direct pumping at 888 nm to reduce the limitation of the large quantum defect [8]. Recently, Li *et al.* reported a highly efficient 1.34  $\mu\text{m}$  laser by end-pumping multisegment Nd:YVO<sub>4</sub> crystal with a wavelength locked laser diode (LD) at 878.6 nm [9]. However, the theoretical analysis in previous works only individually

considered the influence of ETU effect on 1.34  $\mu\text{m}$  laser output and thermal effects, as well as the influence of ESA effect on the thermal effects. More importantly, one may notice that the couplings among the temperature distribution in the laser crystal, the thermal fractional loading, the upper state populations involved in ETU or ESA effect, the laser output and other temperature dependent variables were not taken into account in these works.

In this paper, an internally self-consistent theoretical model was developed considering both ETU and ESA effects, as well as the couplings among the temperature distribution in the laser crystal, the thermal fractional loading, the upper state population involved in the ETU and ESA effects, the laser output and other temperature-dependent parameters. An iteration procedure was employed to introduce the couplings into the theoretical model and simulate the temperature distribution inside the laser crystal, the thermal focal length of the laser crystal and the laser performance. Based on the theoretical and experimental studies of the dependences of the output power and thermal focal length on the boundary temperature of laser crystal, the transmission of the output coupler and the incident pump power, a high power continuous-wave (CW) TEM<sub>00</sub> Nd:YVO<sub>4</sub> 1.34  $\mu\text{m}$  laser dual-end pumped at 880 nm was demonstrated.

## 2. Theoretical analysis considering the influence of ETU and ESA effects

### 2.1. General rate equations model including ETU and ESA effects

The simplified energy level diagram of Nd<sup>3+</sup> ions in YVO<sub>4</sub> crystal involving levels and processes relative to the laser transition at 1.34  $\mu\text{m}$  is shown in Fig. 1 [10]. The pump radiation at 880 nm is absorbed from <sup>4</sup>I<sub>9/2</sub> to <sup>4</sup>F<sub>3/2</sub> (blue solid arrow line in Fig. 1). The laser transition at 1.34  $\mu\text{m}$  takes place between the <sup>4</sup>F<sub>3/2</sub> and <sup>4</sup>I<sub>13/2</sub> levels (red solid arrow line in Fig. 1). The ESA at the laser wavelength (<sup>4</sup>F<sub>3/2</sub> → <sup>4</sup>G<sub>7/2</sub>) and the possible ETU processes designated as UC1-UC4 are denoted by pink and green solid arrow lines, respectively. All dashed arrow lines indicate heat-generation processes.

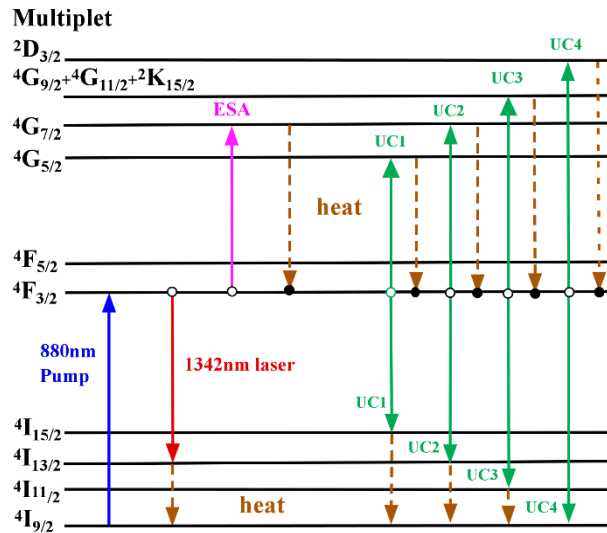


Fig. 1. Energy-level diagram of Nd:YVO<sub>4</sub> involving levels and processes relative to the laser transition at 1.34  $\mu\text{m}$ .

For a 1.34  $\mu\text{m}$  Nd:YVO<sub>4</sub> laser in TEM<sub>00</sub> operation, the space-dependent rate-equations including ETU and ESA effects can be written as [11,12]

$$\frac{dn(x, y, z)}{dt} = R_p r_p(x, y, z) - \frac{c}{n_e} \sigma_e n(x, y, z) \Phi \phi_0(x, y, z) - \frac{n(x, y, z)}{\tau} - \gamma n(x, y, z)^2, \quad (1)$$

$$\frac{d\Phi}{dt} = \frac{c}{n_e} (\sigma_e - \sigma_{esa}^l) \Phi \int_{Crystal} n(x, y, z) \phi_0(x, y, z) dV - \frac{\Phi}{\tau_c}, \quad (2)$$

where  $n(x, y, z)$  is the upper-state population density,  $R_p$  is the pumping rate,  $c$  is the light speed in vacuum,  $n_e$  is the refraction index of laser medium,  $\Phi$  is the total number of laser photons in the cavity.  $\tau$  is the fluorescence lifetime of the upper-state.  $\gamma$  is the ETU parameter.  $\sigma_e$  and  $\sigma_{esa}^l$  are the stimulated emission cross-section and ESA cross-section at the laser wavelength, respectively.  $\tau_c$  is the cavity photon lifetime that can be written as

$$\tau_c = \frac{2l_{eff}}{c} \frac{1}{\delta_0 - \ln(1 - T_{oc})}, \quad (3)$$

where  $l_{eff} = l_c + (n_e - 1)l_0$  is the optical length of laser cavity,  $l_c$  and  $l_0$  are the geometric lengths of the cavity and laser crystal.  $\delta_0$  is the round-trip dissipative loss and  $T_{oc}$  is the transmission of output coupler.  $r_p(x, y, z)$  and  $\phi_0(x, y, z)$  are the normalized spatial distributions of pump and laser photons, respectively. The spatial distribution of pump beam was measured using the knife-edge method [13] in our experiment, and can be well fitted as a super Gaussian function. For dual-end pumping,  $r_p(x, y, z)$  can be given by:

$$r_p(x, y, z) = 2\sqrt{2} \frac{\alpha(\exp(-\alpha(z - \frac{l_0 - l}{2})) + \exp(-\alpha(l - z + \frac{l_0 - l}{2})))}{\left( \Gamma\left[\frac{1}{4}\right] - \Gamma\left[\frac{1}{4}, 2\left(\frac{A_x}{2\omega_{pa}}\right)^4\right] \right) \left( \Gamma\left[\frac{1}{4}\right] - \Gamma\left[\frac{1}{4}, 2\left(\frac{A_y}{2\omega_{pa}}\right)^4\right] \right)} \omega_{pa}^2 \eta_\alpha \times \exp\left[ -2 \left( \left( \frac{x - \frac{A_x}{2}}{\omega_{pa}} \right)^4 + \left( \frac{y - \frac{A_y}{2}}{\omega_{pa}} \right)^4 \right) \right], \quad (4)$$

where  $\eta_\alpha = 1 - \exp(-\alpha l)$  is the pump absorption efficiency,  $\alpha$  and  $l$  are the absorption coefficient and geometric length of the doped portion of laser crystal, respectively.  $A_x$  and  $A_y$  are the lengths of laser crystal along the  $x$  and  $y$  directions on the transverse cross-section, respectively. The laser propagates along the  $z$  direction.  $\Gamma$  is the Gamma function and  $\omega_{pa}$  is the average pump beam radius in the laser crystal. With the assumption that the laser flux is almost constant in the laser cavity,  $\phi_0(x, y, z)$  can be given by

$$\phi_0(x, y, z) = \frac{2}{\pi\omega_0^2 l_{eff}} \exp\left[ -2 \frac{x^2 + y^2}{\omega_0^2} \right], \quad (5)$$

where  $\omega_0$  is the laser beam waist that can be calculated via ABCD matrix method using the parameters of laser cavity and the thermal focal length ( $f_t$ ) of laser crystal.

For CW laser operation,  $n(x, y, z)$  can be derived from Eq. (1) and written as

$$n(x, y, z) = \frac{2R_p r_p(x, y, z)}{\left[ \frac{c}{n_e} \sigma_e \Phi \phi_0(x, y, z) + \frac{1}{\tau} \right] + \left\{ \left[ \frac{c}{n_e} \sigma_e \Phi \phi_0(x, y, z) + \frac{1}{\tau} \right]^2 + 4\gamma R_p r_p(x, y, z) \right\}^{1/2}}. \quad (6)$$

The incident pump power ( $P_{in}$ ) and the laser output ( $P_{out}$ ) are linked to the parameters  $R_p$  and  $\Phi$  by the relationships:

$$R_p = \frac{P_{in} \eta_\alpha}{h\nu_p}, \quad (7)$$

$$P_{out} = \frac{-\ln(1-T_{oc})\Phi ch\nu_l}{2l_{eff}}, \quad (8)$$

where  $h\nu_p$  and  $h\nu_l$  are the energies of pump and laser photons, respectively.

Substituting Eqs. (6)-(8) into Eq. (2) and letting  $d\Phi/dt = 0$ , the relationship between  $P_{in}$  and  $P_{out}$  can be obtained as

$$\int_{Crystal} \frac{2\phi_0(x, y, z)r_p(x, y, z)}{A_1 + \sqrt{A_1^2 + A_2}} dV = \frac{n_e h\nu_p (\delta_0 - \ln(1-T_{oc}))}{2l_{eff} P_{in} (\sigma_e - \sigma_{esa}^l) \eta_\alpha \tau}, \quad (9)$$

where

$$A_1 = \frac{2}{h\nu_l} \frac{\sigma_e \tau}{n_e} \frac{P_{out} l_{eff}}{-\ln(1-T_{oc})} \phi_0(x, y, z) + 1, \quad (10)$$

$$A_2 = \frac{4}{h\nu_p} \gamma \tau^2 P_{in} \eta_\alpha r_p(x, y, z).$$

## 2.2. General model of thermal fractional loading including ETU and ESA effects

For a 1.34  $\mu\text{m}$  Nd:YVO<sub>4</sub> laser, if ETU and ESA effects are considered, these two processes will give rise to an extra heat load in the laser crystal, the fractional thermal loading ( $\xi$ ) can be written as [14]:

$$\xi = \xi_0 + \frac{\lambda_p}{\lambda_l} \frac{N_{etu} + N_{esa}}{N_0}, \quad (11)$$

where  $\xi_0$  is the fractional thermal loading in absence of the ETU and ESA effects,  $N_0 = R_p \tau$  is the population in the upper laser level without the ETU and ESA effects.  $N_{etu}$  and  $N_{esa}$  represent the populations in the upper laser level involved in ETU or ESA effect, respectively, and can be written as:

$$N_{etu} = \tau \gamma \int_{Crystal} n(x, y, z)^2 dV, \quad (12)$$

$$N_{esa} = \frac{c\tau}{n_e} \sigma_{esa}^l \Phi \int_{Crystal} n(x, y, z) \phi_0(x, y, z) dV. \quad (13)$$

In the case that the couplings among the values of the thermal and spectral parameters of the laser crystal and the temperature inside the laser crystal are not taken into account, the thermal focal length of a dual-end diffusion-bonded laser crystal can be calculated using [15]

$$f_{t-i} = \frac{-f_1^2}{l - 2f_1}, \quad (14)$$

where

$$f_1 = \frac{2\pi K_{c,a} \omega_{pa}^2}{\xi P_{in} \eta_\alpha} \frac{1}{dn_e / dT + (n_e - 1) \alpha_T}, \quad (15)$$

where  $K_c$  and  $K_a$  are the thermal conductivities along the  $c$ -axis and  $a$ -axis of laser crystal,  $dn_e/dT$  indicates the thermal-optic coefficient, and  $\alpha_T$  is the thermal expansion coefficient.

### 2.3. Determination of the temperature distribution in the laser crystal and simulations of thermal lensing effect and laser performances

It is well known that the thermal and spectral parameters, such as  $\tau$ ,  $\sigma_e$ ,  $\sigma_{esa}^j$ ,  $\gamma$ ,  $\alpha$ ,  $K_c$ ,  $K_a$ ,  $\alpha_T$ ,  $n_e$ ,  $dn_e/dT$ ,  $N_{etu}$ ,  $N_{esa}$ ,  $\zeta$  and  $f_l$ , are all in themselves functions of temperature. Especially, under high intensity pumping, the temperature in the laser crystal will be raised up significantly and nonuniformly distributed, and the values of parameters mentioned above will be changed with the temperature. Conversely, the change of parameters' values will affect the temperature value and distribution in the laser crystal. For example, the ETU parameter will be increased with the rising of the temperature in the laser crystal, which makes a rise of the fraction of heat extraction from the absorbed pump energy and heightens the temperature in the laser crystal. For this reason, the couplings among the values of parameters mentioned above and the temperature inside the laser crystal should be introduced into the model presented in subsections 2.1 and 2.2 with an iteration method when the laser behaviors and the thermal lensing effects are simulated. In this subsection, based on giving the general model of the temperature distribution inside the laser crystal and the temperature dependences of the thermal and spectral parameters, a detailed iteration procedure is proposed and used to simulate the temperature distributions inside the laser crystal with and without the effects of ETU and ESA, respectively.

In general, the spatial temperature distribution inside the dual-end-pumped cubic Nd:YVO<sub>4</sub> crystal can be obtained by solving the following steady state heat equation [16]:

$$K_c \frac{\partial^2 T(x, y, z)}{\partial x^2} + K_a \frac{\partial^2 T(x, y, z)}{\partial y^2} + K_a \frac{\partial^2 T(x, y, z)}{\partial z^2} = -\xi P_m \eta_a r_p(x, y, z). \quad (16)$$

Considering the case that the pumped front and back end faces of the laser crystal are exposed to ambient air with a constant temperature  $T_a$ , and the four lateral faces are in close thermal contact with a heat sink which is temperature controlled at  $T_b$ , the boundary conditions can be written as:

$$K_a \left. \frac{\partial T}{\partial z} \right|_{z=0} = H [T(z=0) - T_a], \quad (17)$$

$$-K_a \left. \frac{\partial T}{\partial z} \right|_{z=l_0} = H [T(z=l_0) - T_a], \quad (18)$$

$$T(x=0, A_x) = T(y=0, A_y) = T_b, \quad (19)$$

where  $H$  is the heat transfer coefficient between crystal and air.

The temperature dependences of  $K_c$  and  $K_a$  of Nd:YVO<sub>4</sub> crystal are described as [17]:

$$K_c = K_{c,g} \frac{T_g}{T}, \quad K_a = K_{a,g} \frac{T_g}{T}, \quad (20)$$

where  $K_{c,g}$  and  $K_{a,g}$  are the thermal conductivities along the  $c$ -axis and  $a$ -axis of the laser crystal at a given temperature  $T_g$ . For Nd:YVO<sub>4</sub> crystal, typically,  $K_{c,g} = 5.23$  W/m·K and  $K_{a,g} = 5.10$  W/m·K at  $T_g = 300$  K.

The temperature dependence of  $\alpha_T$  of Nd:YVO<sub>4</sub> crystal is described as [18]:

$$\alpha_T = (-0.60786 + 0.00896 * T) * 10^{-6} (\text{K}^{-1}). \quad (21)$$

The temperature dependences of  $\eta_\alpha$  and  $r_p(x,y,z)$  are mainly relied on the relationship between  $\alpha$  and  $T$ . For a Nd:YVO<sub>4</sub> crystal with the doping concentration of 0.27 at.% that was used in our experiment, the relationship between  $\alpha$  and  $T$  was obtained by linearly fitting the measured values of  $\alpha$  that were obtained under different crystal temperatures with a collimated pump beam single passing through the crystal, which is

$$\alpha = 3.88 * 10^{-4} * T + 1.408 \text{ (cm}^{-1}\text{)}. \quad (22)$$

To simulate the  $\xi$  versus  $T$  relation, the temperature dependences of  $n_e$ ,  $\tau$ ,  $\sigma_e$ ,  $\sigma_{esa}^J$  and  $\gamma$  are required. The relationship between  $n_e$  and  $T$  is given as [19]:

$$n_e = 2.15478 + 0.72 * 10^{-5} * (T - 296) + 0.309 * 10^{-8} * (T - 296)^2. \quad (23)$$

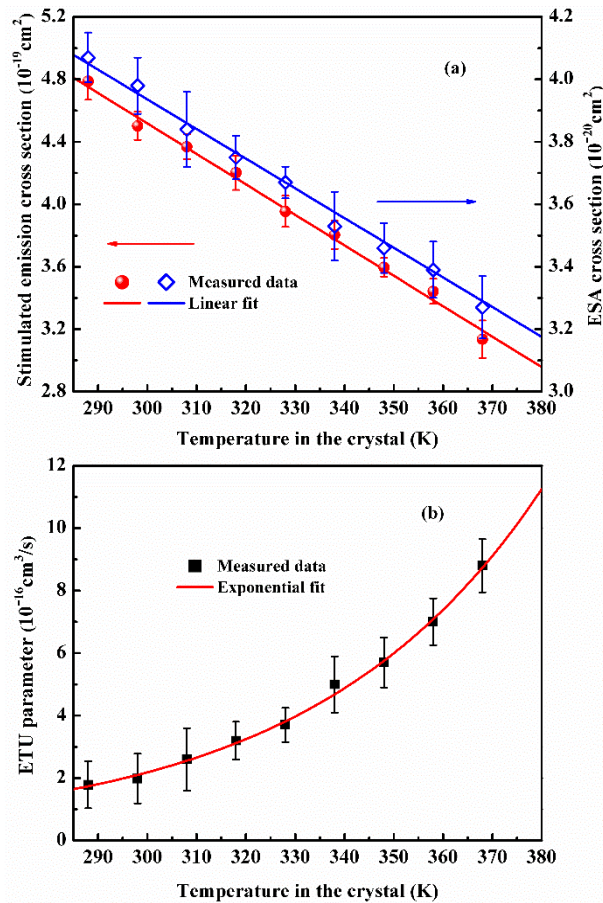


Fig. 2. Temperature dependences of (a) stimulated emission cross-section and ESA cross-section, (b) ETU parameter.

The relationship between  $\tau$  and  $T$  is given by fitting the experimental data in [20] with a single-exponential function based on the method in [21]:

$$\tau(T) = \frac{1 + \exp(-25.9156/T)}{1/90.3 + (1/107.1)\exp(-25.9156/T)} \text{ (}\mu\text{s)}. \quad (24)$$

Figure 2(a) shows the measured  $\sigma_e$  and  $\sigma_{esa}^J$  at peak wavelength of stimulated emission spectrum using the method in [22]. The relationships between  $\sigma_e$ ,  $\sigma_{esa}^J$  and  $T$  were obtained by linearly fitting the measured data, which are

$$\sigma_e(T) = 10.3675 \times 10^{-19} (\text{cm}^2) - 1.95 \times 10^{-21} (\text{cm}^2 / \text{K}) \times T, \quad (25)$$

$$\sigma_{esa}^l(T) = 0.6786 \times 10^{-19} (\text{cm}^2) - 0.095 \times 10^{-21} (\text{cm}^2 / \text{K}) \times T. \quad (26)$$

Moreover, the temperature dependence of  $\gamma$  can be determined via the method in [23] and using the measured spectra of stimulated-emission, stimulated-absorption and ESA. Using the measured data shown in Fig. 2(b), the relationship between  $\gamma$  and  $T$  can be fitted as

$$\gamma(T) = [3.054 \times \exp(0.02156 \times T) + 217.63] \times 10^{-19} (\text{cm}^3 / \text{s}). \quad (27)$$

Due to the temperature distribution inside the laser crystal is nonuniform, the laser beam passing through the laser crystal will experience an optical path difference (OPD) as [24]

$$\text{OPD}(x, y) = \int_0^l \left[ \frac{dn_e}{dT} + (n_e - 1) \alpha_T \right] T(x, y, z) dz. \quad (28)$$

Since the temperature distribution is approximate parabolic inside the pumped region in the laser crystal, the relationship between the thermal focal length of laser crystal and  $T$  can be determined by [24]

$$f_t = \frac{2\omega_{pa}^2}{\text{OPD}(A/2, A/2) - \text{OPD}(A/2 + 2\omega_{pa}, A/2 + 2\omega_{pa})}. \quad (29)$$

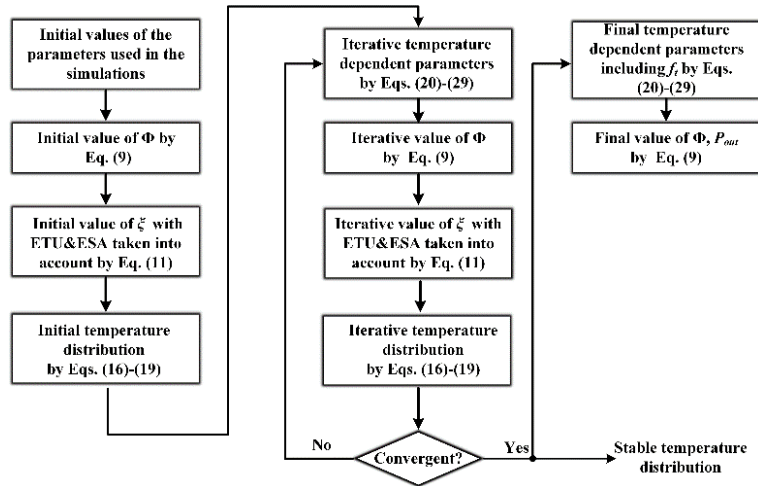


Fig. 3. Iteration procedure used for the simulations of the temperature distribution inside the laser crystal, the thermal focal length of laser crystal and laser performance.

In order to introduce the couplings among the thermal and spectral parameters and the temperature inside the laser crystal into the theoretical model, an iteration procedure is employed to simulate the temperature distribution inside the laser crystal, the thermal focal length and laser performance, as shown in Fig. 3. In the first step of iteration procedure, an initial temperature distribution in the laser crystal is obtained by assigning the thermal and spectral parameters as their values at the temperature of  $T_b$ , calculating the initial values of  $\Phi$ ,  $\zeta$  and  $f_t$  by Eq. (9), Eq. (11), and Eq. (14), respectively. In the second step of iteration procedure, the temperature distribution in the laser crystal is iteratively calculated by assigning the thermal and spectral parameters as three-dimension matrixes that are derived based on the spatial temperature distribution obtained in previous iteration, calculating the iterative values of  $\Phi$ ,  $\zeta$  and  $f_t$  by Eq. (9), Eq. (11), and Eq. (29), respectively. The iteration is carried out repeatedly, until the iterative error, which is defined as the difference of the

maximum temperature between two adjacent iterations [25], is less than 0.01 K. A stable temperature distribution in the laser crystal is achieved. In the third step, the values of  $\Phi$ ,  $\xi$ ,  $f_i$  and  $P_{out}$  can be obtained based on the stable spatial temperature distribution in the laser crystal.

For a dual-end-pumped 1.34  $\mu\text{m}$   $\text{YVO}_4\text{-Nd:YVO}_4\text{-YVO}_4$  laser with a plane-plane cavity configuration, in which the laser crystal is very close to one of the cavity mirrors, the spatial temperature distribution in the laser crystal, the thermal focal length of laser crystal and the 1.34  $\mu\text{m}$  laser performance were simulated by the iteration procedure shown in Fig. 3 and the parameters:  $\lambda_p = 880$  nm,  $\lambda_l = 1342$  nm,  $\omega_{pa} = 510$   $\mu\text{m}$ ,  $\delta_0 = 0.015$ ,  $l_{eff} = 126$  mm,  $l_0 = 27$  mm,  $l = 17$  mm,  $T_a = 298$  K,  $T_b = 288$  K,  $A_x = A_y = 3$  mm,  $H = 10$  W/m<sup>2</sup>K,  $T_{oc} = 10\%$ , and  $P_{in} = 50$  W.

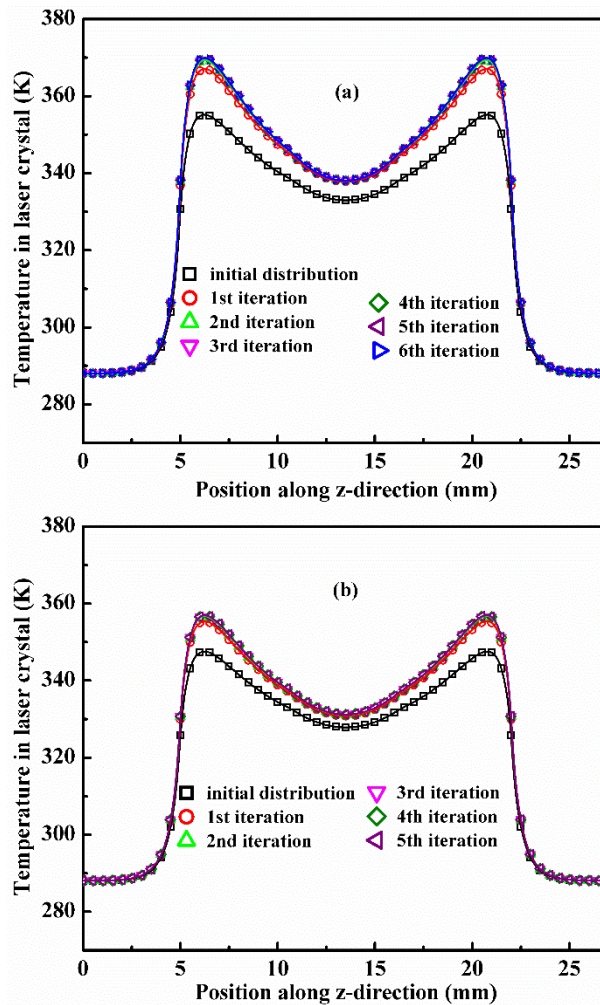


Fig. 4. Simulated temperature distributions at  $x = y = 1.5$  mm along  $z$ -direction (a) with and (b) without the effects of ETU and ESA taken into account.

Figures 4(a) and 4(b) are the simulated temperature distributions at  $x = y = 1.5$  mm in the laser crystal with and without the effects of ETU and ESA taken into account, respectively. It can be seen, when the effects of ETU and ESA are taken into account, the iterative error is 0.005 K after carrying out the iteration for 6 times and the maximum temperature inside the laser crystal is 369.945 K. As a comparison, when the effects of ETU and ESA are ignored,

the iterative error is 0.005 K after carrying out the iteration for 5 times and the maximum temperature inside the laser crystal is 356.977 K.

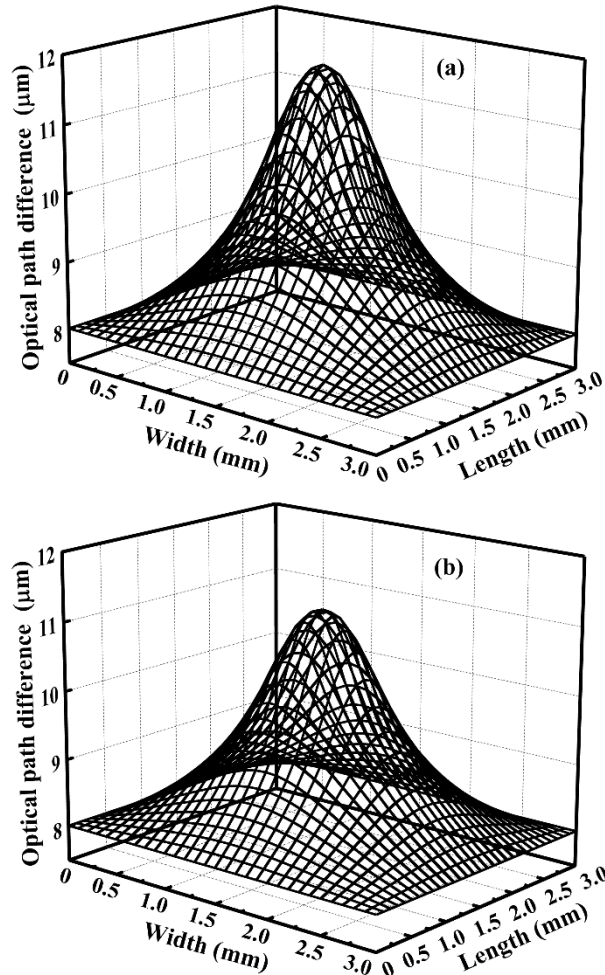


Fig. 5. Simulated distributions of OPD (a) with and (b) without the effects of ETU and ESA taken into account.

Figures 5(a) and 5(b) show the simulated distributions of OPDs of the laser in the laser crystal with and without the effects of ETU and ESA, respectively. It can be seen, when the effects of ETU and ESA are considered, the value of OPD at the center of the pump region, i.e.  $OPD(A_x/2, A_y/2)$ , is 11.893  $\mu\text{m}$ , while the value at the border of the pump region, i.e.  $OPD(A_x/2 + 2\omega_{pa}, A_y/2 + 2\omega_{pa})$ , is 8.359  $\mu\text{m}$ . As a comparison,  $OPD(A_x/2, A_y/2)$  and  $OPD(A_x/2 + 2\omega_{pa}, A_y/2 + 2\omega_{pa})$  are reduced to 11.216  $\mu\text{m}$  and 8.311  $\mu\text{m}$ , respectively, when the effects of ETU and ESA are not considered. According to Eq. (29), the value of thermal focal length of laser crystal with the effects of ETU and ESA is 0.82 times shorter than that without the effects of ETU and ESA.

The difference of thermal lensing effect shown in Fig. 5 can be attributed to the extra heat deposition originated from the nonradiative transitions of the upper state population involved in ETU and ESA ( $N_{etu} + N_{esa}$ ). Moreover, the existence of  $N_{etu} + N_{esa}$  will reduce the upper-state population density and the total number of laser photons in the cavity. Figure 6 shows the relationships between  $(N_{etu} + N_{esa})/N_0$  and  $T_b$  at different  $T_{oc}$ . It can be seen, the value of  $(N_{etu} + N_{esa})/N_0$  can be reduced with lowering the boundary temperature of laser crystal and

reduced faster with larger  $T_{oc}$ . In particular, when  $T_b = 288$  K,  $(N_{etu} + N_{esa})/N_0$  are 6.36%, 6.63% and 7.05% at  $T_{oc} = 15\%$ , 10% and 5%, respectively. Consequently, the thermal fractional loadings at these three cases with the effects of ETU and ESA taken into account are 38.6%, 38.7% and 39.0%, while that is 34.4% in absence of ETU and ESA effects.

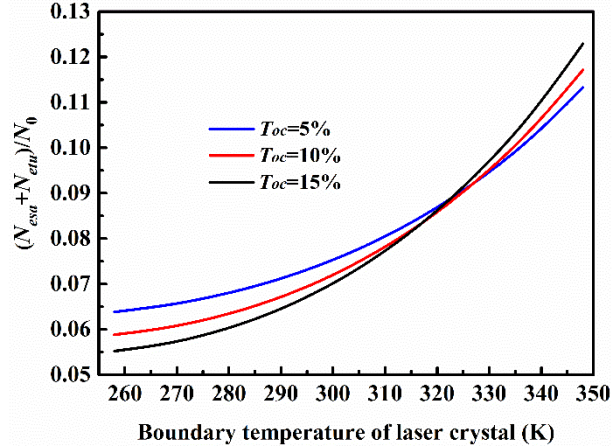


Fig. 6. Simulated relationships between  $(N_{etu} + N_{esa})/N_0$  and  $T_b$  at different  $T_{oc}$ .

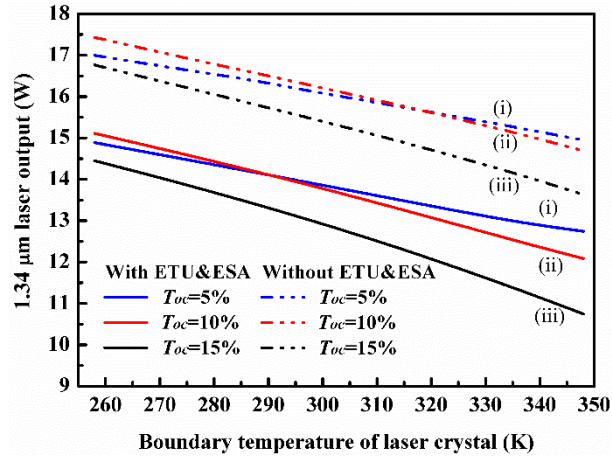


Fig. 7. Simulated relationships between laser output and  $T_b$  at different  $T_{oc}$ .

Figure 7 shows the relationships between  $P_{out}$  and  $T_b$  at different  $T_{oc}$ , where the curves (i), (ii) and (iii) indicate the case of using an output coupler with  $T_{oc} = 5\%$ , 10% and 15%, respectively. Solid and dashed curves correspond to the laser outputs with and without ETU and ESA effects, respectively. It can be seen, the laser output considering ETU and ESA effects is reduced in comparison with that without ETU and ESA effects. The laser output decreases with rising temperature of laser crystal and there exists an optimum output transmission to get the highest output power at a given temperature. According to the theoretical predictions, the laser performance can be optimized by reducing the temperature of laser crystal and using an output coupler with optimum transmission.

### 3. Experimental setup

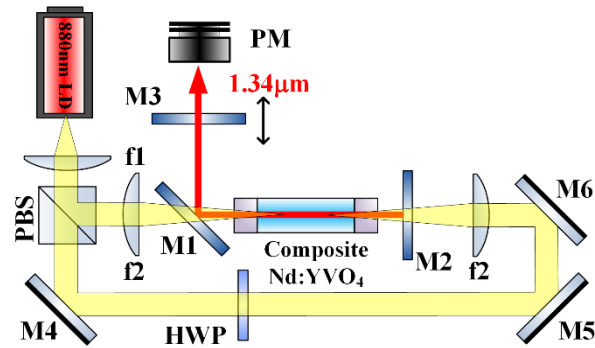


Fig. 8. Experimental setup of a diode-end-pumped 1.34  $\mu\text{m}$  Nd:YVO<sub>4</sub> laser

The experimental setup of a diode-end-pumped 1.34  $\mu\text{m}$  Nd:YVO<sub>4</sub> laser is depicted in Fig. 8. The pump source we used is a fiber-coupled LD (LIMO120-F400-DL880-EX1124, LIMO) with center wavelength of 880 nm, maximum output power of 120 W and core diameter of 400  $\mu\text{m}$ . The gain medium is a composite Nd:YVO<sub>4</sub> crystal consisting of a 17 mm long 0.27 at.% Nd-doped central portion and two 5 mm long undoped end caps. Both end faces are polished and anti-reflection coated at 1.34  $\mu\text{m}$ , 1.06  $\mu\text{m}$  and 880 nm ( $R < 0.2\%$  at all wavelengths). In order to further reduce the temperature of laser crystal and weaken the influence of ETU and ESA effects, a polarized and dual-end pumping scheme is used by employing a collimating lens (f1), a polarizing beam splitter (PBS), a half-wave plate (HWP) and two focusing lenses (f2). The comparison experiment using single-end pumping scheme was realized by blocking the pump beam on right hand side. To investigate the influence of laser crystal boundary temperature on the laser performance, the Nd:YVO<sub>4</sub> crystal is tightly wrapped with indium foil and mounted in a copper block which is temperature controlled precisely by a temperature controller with the accuracy of  $\pm 0.01^\circ\text{C}$  (YG-3D, Yuguang). The laser resonator is a standing-wave cavity formed by three plane mirrors (M1, M2, and M3). To suppress the 1.06  $\mu\text{m}$  transition, two input couplers (M1 and M2) are coated for high transmission at both 880 nm and 1.06  $\mu\text{m}$  ( $T > 95\%$ ) and high reflection ( $R > 99.8\%$ ) at 1.34  $\mu\text{m}$ . The output coupler (M3) is partial transmission coated that will be optimized in the experiment to mitigate the effects of ETU and ESA and improve the laser performance. The length between M2 and the end face of laser crystal is 1 mm. The cavity length can be changed by controlling the position of M3 using a stepper motor permitting a translation movement along the longitudinal direction. The thermal focal length of the laser crystal can be measured by increasing the incident pump power for a given cavity length. When the incident pump power reaches a critical value, the laser cavity will be unstable due to the thermal lens and the laser output is quenched. Based on the experimental results in the research of thermal focal length, the cavity length (geometric length) was fixed at 93 mm when the laser performance was optimized.

### 4. Experimental results and discussions

Figure 9 depicts the measured thermal focal lengths of laser crystal and theoretical predictions with respect to the incident pump power for the two types of pumping scheme at different boundary temperatures of laser crystal. The symbols in Fig. 9 are experimental data. Curves in Fig. 9 are theoretical simulations using the theoretical model in Section 2. The theoretical predictions considering both ETU and ESA effects are in good agreement with experimental results. The value of thermal focal length will show a 24 mm increase when the boundary temperature is reduced from 318 K to 288 K under dual-end pumping and an incident pump power of 50 W. As a comparison, the thermal focal length is significantly

shorter when the single-end pumping is used, as shown in Fig. 9 (black squares and curve). Obviously, the thermal lensing effect can be weakened using dual-end pumping scheme and lower boundary temperature of laser crystal.

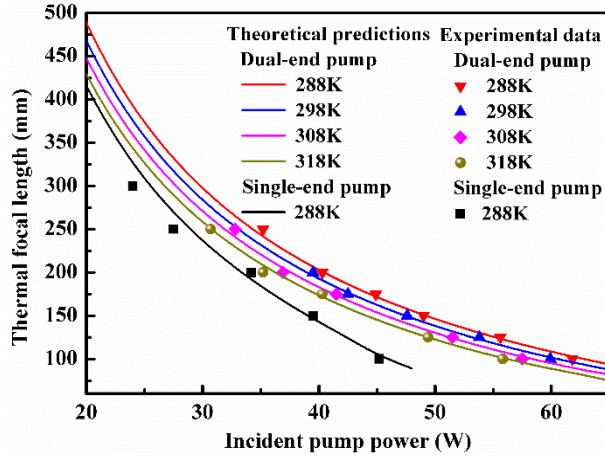


Fig. 9. Thermal focal length of laser crystal versus incident pump power at different pump schemes and boundary temperatures of laser crystal.

When the geometric cavity length was fixed as 93 mm and output coupler with the transmission of 10% was used, the 1.34  $\mu\text{m}$  laser output was measured by a power meter (*LabMax-TOP*, Coherent). Figure 10 shows the 1.34  $\mu\text{m}$  laser output as a function of the incident pump power for the two pumping schemes at different boundary temperatures of laser crystal. The measured maximum output power was 16 W when the boundary temperature of laser crystal was 288 K at dual-end pumping scheme with a total pump power of 60 W. By contrast, the measured maximum output power was 11 W at single-end pumping scheme. It can be seen, the output power was reduced with rising boundary temperature of laser crystal.

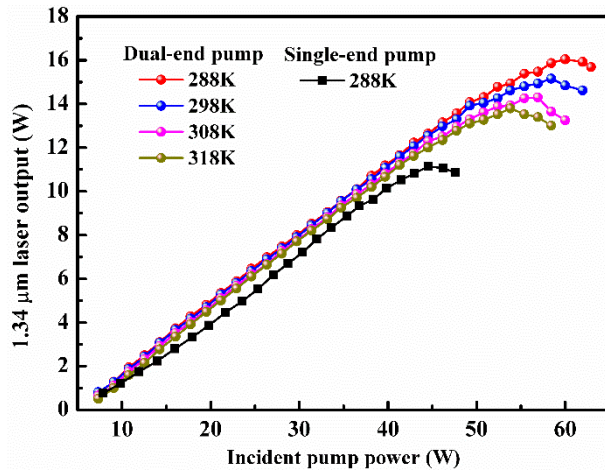


Fig. 10. Output power of 1.34  $\mu\text{m}$  laser versus incident pump power at different pump schemes and boundary temperatures of laser crystal.

Figure 11 shows the 1.34  $\mu\text{m}$  laser output as a function of boundary temperatures of laser crystal at a pump power of 50 W under dual-end pumping. Circles in Fig. 11 are the experimental data. Solid and dashed curves in Fig. 11 are the theoretical predictions with and

without both ETU and ESA effects, respectively. The 1.34  $\mu\text{m}$  output power was increased from 13.2 W to 14.2 W when the boundary temperature of laser crystal was reduced from 318 K to 288 K. The theoretical prediction considering both ETU and ESA effects is in good agreement with experimental results.

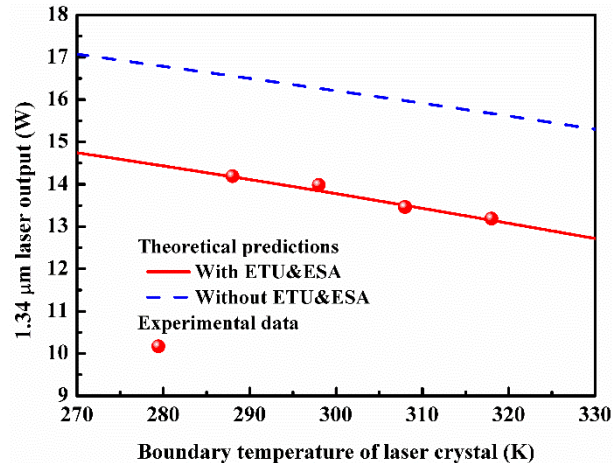


Fig. 11. 1.34  $\mu\text{m}$  output power versus boundary temperatures of laser crystal under dual-end pumping.

Figure 12 shows the dependences of the 1.34  $\mu\text{m}$  laser output on transmission of output coupler at a boundary temperature of 288 K and an incident pump power of 50 W under dual-end pumping. The circles are experimental data. The red solid curve is the theoretical prediction considering both ETU and ESA effects that are in good agreement with experimental results. As a comparison, the blue dashed curve is the theoretical prediction without both ETU and ESA effects that deviate significantly from experimental results. It can be seen, there exists an optimum output transmission to achieve a maximum laser output. When ETU and ESA effects are considered the optimum transmission of output coupler is 6.7%, but it should be 7.8% when ETU and ESA effects are neglected.

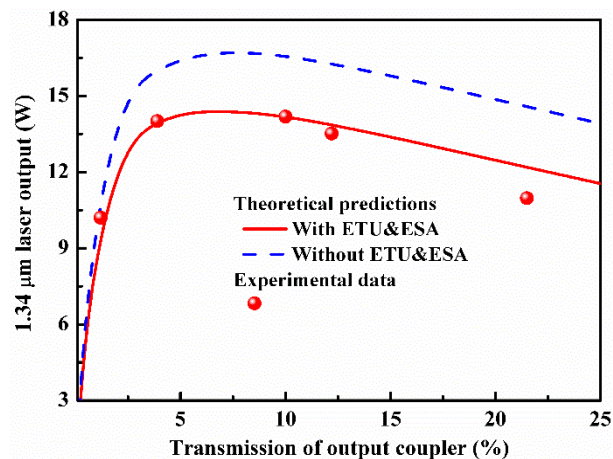


Fig. 12. 1.34  $\mu\text{m}$  output power versus transmission of output coupler.

When the dual-end pumping scheme was used, the boundary temperature of laser crystal was controlled at 288 K and the output transmission was 10%, a CW TEM<sub>00</sub> 1.34  $\mu\text{m}$  laser with output power of 16 W was obtained at an incident pump power of 60 W. The laser beam

quality was measured using a beam analyzer (DataRay, BMS2-4XY) and found to be  $M_x^2 = M_y^2 = 1.17$ . The power stability of the 1.34  $\mu\text{m}$  laser at an average output power around 16 W was measured by the power meter and recorded by a computer as shown in Fig. 13. The stability of the laser output was better than  $\pm 0.9\%$  for a given four hours.

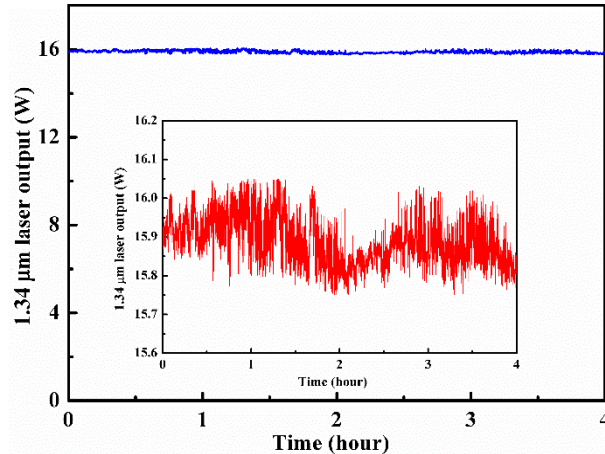


Fig. 13. Stability of 1.34  $\mu\text{m}$  laser output.

## 5. Conclusions

We presented a detailed investigation on the behaviors of 1.34  $\mu\text{m}$  Nd:YVO<sub>4</sub> lasers and its thermal lensing effects with particular attention given to the influences of ETU and ESA effects. An internally self-consistent theoretical model was developed considering both ETU and ESA effects, as well as the couplings among the temperature distribution in the laser crystal, the thermal fractional loading, the upper state population involved in the ETU and ESA effects, the laser output and other temperature-dependent parameters. In order to introduce the couplings into the theoretical model, an iteration procedure was employed to simulate the temperature distribution inside the laser crystal, the thermal focal length of the laser crystal and the laser performance. Based on the fabrication of a high power CW TEM<sub>00</sub> Nd:YVO<sub>4</sub> 1.34  $\mu\text{m}$  laser dual-end pumped at 880 nm, the dependences of the output power and thermal focal length on the boundary temperature of laser crystal, the transmission of output coupler and the incident pump power were studied theoretically and experimentally. When the dual-end pumping scheme was used, the boundary temperature of laser crystal was controlled at 288 K and the output transmission was 10%, a CW TEM<sub>00</sub> 1.34  $\mu\text{m}$  laser with measured maximum output power of 16 W was obtained at an incident pump power of 60 W. The measured laser beam quality was  $M_x^2 = M_y^2 = 1.17$  and the stability of the laser output was better than  $\pm 0.9\%$  for a given four hours. The good agreement obtained between experimental results and theoretical predictions considering both ETU and ESA effects confirms our analysis and constitutes a direct validation of our model. The investigation is helpful to improve the output performance of 1.34  $\mu\text{m}$  lasers that can be widely used in applications, such as fiber telecommunication, fiber sensing, medical treatment and scientific research.

## Funding

Key Project of the Ministry of Science and Technology of China (2017YFB0405203).